J Pathol Inform

Editor-in-Chief:
Anil V. Parwani , Pittsburgh, PA, USA
Liron Pantanowitz, Pittsburgh, PA, USA

OPEN ACCESS
HTML format

For entire Editorial Board visit : www.jpathinformatics.org/editorialboard.asp

Technical Note

TissueCypher™: A systems biology approach to anatomic pathology

Jeffrey W. Prichard[1], Jon M. Davison[2], Bruce B. Campbell[3], Kathleen A. Repa[3], Lia M. Reese[3], Xuan M. Nguyen[3], Jinhong Li[1], Tyler Foxwell[2], D. Lansing Taylor[4], Rebecca J. Critchley-Thorne[3]

[1]Department of Pathology and Laboratory Medicine, Geisinger Medical Center, Danville, PA 17822, [2]Department of Pathology, University of Pittsburgh Medical Center, Pittsburgh, PA 15213, [3]Cernostics, Inc., 235 William Pitt Way, Pittsburgh, PA 15238, [4]Department of Computational and Systems Biology, Drug Discovery Institute, University of Pittsburgh, Pittsburgh, PA 15260, USA

E-mail: *Rebecca J. Critchley-Thorne - rthorne@cernostics.com
*Corresponding Author

Received: 18 May 2015 Accepted: 31 July 2015 Published: 31 August 2015

Abstract

Background: Current histologic methods for diagnosis are limited by intra- and inter-observer variability. Immunohistochemistry (IHC) methods are frequently used to assess biomarkers to aid diagnoses, however, IHC staining is variable and nonlinear and the manual interpretation is subjective. Furthermore, the biomarkers assessed clinically are typically biomarkers of epithelial cell processes. Tumors and premalignant tissues are not composed only of epithelial cells but are interacting systems of multiple cell types, including various stromal cell types that are involved in cancer development. The complex network of the tissue system highlights the need for a systems biology approach to anatomic pathology, in which quantification of system processes is combined with informatics tools to produce actionable scores to aid clinical decision-making. **Aims:** Here, we describe a quantitative, multiplexed biomarker imaging approach termed TissueCypher™ that applies systems biology to anatomic pathology. Applications of TissueCypher™ in understanding the tissue system of Barrett's esophagus (BE) and the potential use as an adjunctive tool in the diagnosis of BE are described. **Patients and Methods:** The TissueCypher™ Image Analysis Platform was used to assess 14 epithelial and stromal biomarkers with known diagnostic significance in BE in a set of BE biopsies with nondysplastic BE with reactive atypia (RA, *n* = 22) and Barrett's with high-grade dysplasia (HGD, *n* = 17). Biomarker and morphology features were extracted and evaluated in the confirmed BE HGD cases versus the nondysplastic BE cases with RA. **Results:** Multiple image analysis features derived from epithelial and stromal biomarkers, including immune biomarkers and morphology, showed significant differences between HGD and RA. **Conclusions:** The assessment of epithelial cell abnormalities combined with an assessment of cellular changes in the lamina propria may serve as an adjunct to conventional pathology in the assessment of BE.

Key words: Barrett's esophagus, biomarkers, computer vision, digital pathology, high-grade dysplasia, multiplexed immunofluorescence, quantitative image analysis, reactive atypia, stromal cells, TissueCypher™

Access this article online

Website: www.jpathinformatics.org

DOI: 10.4103/2153-3539.163987

Quick Response Code:

INTRODUCTION

The majority of tissue-based diagnoses are made by manual analysis of hematoxylin and eosin

This is an open access article distributed under the terms of the Creative Commons Attribution-NonCommercial-ShareAlike 3.0 License, which allows others to remix, tweak, and build upon the work non-commercially, as long as the author is credited and the new creations are licensed under the identical terms.

For reprints contact: reprints@medknow.com

This article may be cited as:
Prichard JW, Davison JM, Campbell BB, Repa KA, Reese LM, Nguyen XM, *et al.* TissueCypher™: A systems biology approach to anatomic pathology. J Pathol Inform 2015;6:48.

Available FREE in open access from: http://www.jpathinformatics.org/text.asp?2015/6/1/48/163987

(H&E)-stained slides by light microscopy. When biomarkers are assessed, they are typically labeled by immunohistochemistry (IHC) with manual interpretation. While these traditional pathology methods are valuable, they are limited by subjectivity, variability, and workflow inefficiencies. Digital pathology is gaining momentum with the adoption of high-throughput whole slide scanners to digitize tissue slides,[1-3] and algorithms for automated histologic grading and semi-quantitative assessment of biomarkers stained by IHC.[4-8] The Food and Drug Administration (FDA) has approved some of these algorithms for *in vitro* diagnostic use.[9,10] This transition to a digital workflow will improve efficiency and objectivity, however, even with digital slide analysis the accuracy of chromogenic IHC is limited by inherent variability in staining intensity and multiplexing of IHC is challenging. Furthermore, the majority of biomarkers used in anatomic pathology are markers of epithelial cell processes. The structure of the tissue system and the vital interactions of epithelial cells with stromal components, including multiple types of immune cells, demonstrate the need for a systems biology approach to anatomic pathology testing.[11,12] Assessment of tumors and premalignant tissues as a "system" has the potential to improve on the current diagnostic tools by creating high content profiles that capture key features of the tissue environment, and quantify both genetic and nongenetic heterogeneity. This tissue systems approach termed "TissueCypher™" is the subject matter of multiple issued patents and patent applications.[13-16]

Technologies that measure changes in gene expression or mutations require tissues to be digested to extract nucleic acids, resulting in loss of morphology and spatial data that are critical for accurate measurement and interpretation of many biomarkers. Therefore, a spatial systems biology approach is required that builds on standard pathology methods to measure multiple key biomarkers in the appropriate context of tissue architecture.

TissueCypher™ is a platform for multi-channel fluorescence whole slide digital image reading, image object segmentation and high-dimensional biomarker and morphology feature measurements. This is coupled to classifier software to integrate biomarker data with morphology data and clinical data to produce diagnostic, prognostic and predictive scores. The TissueCypher™ approach has broad applications in anatomic pathology, particularly in disease areas where there is significant observer variability, where tissue sample volume is limited, and where multiple biomarkers are required for accurate assessment of diagnosis, prognosis or response to therapies.[13-16]

Barrett's esophagus (BE) surveillance is one such area in which there is significant variability in the histologic diagnosis of premalignant stage, and limited biopsy material available for analysis of multiple biomarkers assessed by traditional IHC methods.[17,18] BE develops in a background of chronic inflammation and both epithelial and stromal processes play a role in disease progression. BE is a precursor to esophageal adenocarcinoma (EAC), which develops in a defined sequence of changes from benign metaplasia, to low grade dysplasia (LGD), to high grade dysplasia (HGD) to EAC. The risk of progression to EAC is very low,[19-21] however, treatment options for EAC are limited and thus early detection is critical. Patients with BE are frequently screened by endoscopy with biopsies and management decisions are based on histologic evaluation of esophageal biopsies by pathologists.[22] The difficulties in accurately diagnosing dysplasia in BE by morphology alone has been well-described.[23,24] Pathology analyses are frequently confounded by ambiguous cases, such as reactive atypia (RA) and dysplasia, which can appear morphologically similar, but have very different clinical outcome and require different management. RA is believed to reflect epithelial regeneration in response to inflammation and does not indicate increased risk of cancer. Dysplasia, particularly when high-grade, is the morphologic manifestation of neoplastic transformation and is associated with a high risk of cancer. Current clinical guidelines recommend intervention with endoscopic ablative therapy for confirmed HGD[22] and there is growing evidence to support ablative therapy for confirmed LGD.[25,26] The histologic differences between dysplastic and reactive epithelia can be subtle and subject to observer variability, particularly in a background of inflammation, adjacent to ulcers or erosions and in mucosa near the junction between squamous and columnar tissue. For example, both dysplastic and reactive epithelium exhibit nuclear changes such as hyperchromasia, however, the atypia is usually more variable in reactive versus dysplastic epithelium. Further, both dysplastic and reactive epithelia display enlarged nuclei, however, dysplasia is associated with irregular nuclear contours whereas reactive nuclei typically have regular nuclear contours.[27,28] These histologic abnormalities form a continuous spectrum and while some cases can be confidently diagnosed, it can be difficult to define a precise line of demarcation between dysplasia and RA. Diagnostic uncertainty is exacerbated by the need to interpret limited samples in small biopsies. Both genetic- and protein-based biomarkers have been shown to contribute to diagnostic accuracy in BE[29-32] and have the potential to aid pathologists in the distinction of regenerative epithelium and dysplasia. However, the difficulties in managing multiple IHC tests on small biopsies and in manually integrating morphologic and molecular findings into a diagnosis have hindered the clinical use of biomarkers in BE. There is no single biomarker that can accurately diagnose the grade of dysplasia of BE[33] and it is clear that a multi-biomarker approach is required. The TissueCypher™ platform will

enable quantitative measurement of multiple epithelial and stromal biomarkers in the context of BE morphology. The TissueCypher™ approach provides the ability to integrate the results of multiple biomarkers on small tissue samples while meeting both the need for improved objectivity in BE diagnostic testing and the need to extract the key molecular and spatial information from the "tissue system" for accurate diagnosis and prognosis. This approach can be applied as an adjunctive tool to conventional pathological analysis to improve objectivity and accuracy in the assessment of BE and enable targeting of ablative therapies to patients with dysplasia. Here, we describe the TissueCypher™ image analysis methods and evaluate the applications of the technology in distinguishing HGD from RA in BE.

PATIENTS AND METHODS

BE cases with gastrointestinal (GI) subspecialist-confirmed diagnoses of nondysplastic BE with RA (RA, n = 22 patients) and BE with HGD (HGD, n = 17 patients) were retrieved from two institutions with accompanying clinicopathological data. The biopsies with RA were from patients with at least 4 years endoscopic surveillance data showing no subsequent disease progression. The biopsies with HGD were from patients with endoscopic surveillance data demonstrating disease progression to either confirmed adenocarcinoma (n = 14) or HGD suspicious for adenocarcinoma (n = 3). The clinicopathological data elements included the original diagnoses provided by a generalist pathologist as part of endoscopic surveillance. Of the 22 cases with GI subspecialist diagnosis of RA, the original diagnoses were LGD (n = 5), indefinite for dysplasia (n = 10) and nondysplastic (n = 7). Of the 17 cases with subspecialist diagnosis of HGD, the original diagnoses were HGD (n = 13), LGD (n = 1), indefinite for dysplasia (n = 1) and nondysplastic (n = 2). The study was approved by the institutional review boards at each institution.

Fluorescence Immunolabeling

Five-micrometer sections of formalin-fixed paraffin-embedded (FFPE) Barrett's biopsies were stained with H&E by standard histology methods. Additional sections were labeled by multiplexed immunofluorescence for cytokeratin 20 (CK-20), Ki-67, β-catenin, p16, alpha-methylacyl-coenzyme A racemase (AMACR), p53, human epidermal growth factor receptor-2/neu (HER2/neu), CDX-2, CD68, nuclear factor kappa-B (NF-κB) p65, cyclooxygenase-2 (COX-2), hypoxia-inducible factor-1 alpha (HIF-1α), CD45RO, CD1a plus Hoechst to label nuclei. The panel of biomarkers evaluated is summarized in Table 1 and includes epithelial-type biomarkers as well as biomarkers of stromal processes such as angiogenesis and specific immune cell subsets, e.g., macrophages. The biomarkers were selected to demonstrate the ability of the TissueCypher Image Analysis Platform to detect systems molecular and cellular changes between different disease states in the spectrum of BE. The biomarkers were multiplexed in four-channel fluorescence sub-panels consisting of Hoechst and three biomarkers per slide. Briefly, slides were baked for 30 min at 60°C, dewaxed by immersion in Aqua DePar (Biocare Medical, Concord, CA), followed by epitope retrieval in Tris-ethylenediaminetetraacetic acid pH 9 buffer at 97–99°C for 30 min then room temperature for 20 min. Slides were then washed, blocked first with Image-iT FX Signal Enhancer (Life Technologies, Carlsbad, CA)

Table 1: Biomarkers evaluated by TissueCypher

Biomarker	Process/function	Abnormality/expression pattern in BE	Selected literature
p53	Tumor suppressor, apoptosis	Nuclear overexpression or loss in epithelial cells	[34,35]
p16	Cell cycle control	Cellular loss in epithelial cells	[31,36]
β-catenin	Adhesion, migration	Nuclear translocation in epithelial cells	[37,38]
HER2/neu	Cell growth, proliferation	Plasma membrane overexpression in epithelial cells	[39,40]
AMACR	Lipid metabolism	Overexpression in peroxisomes and mitochondria of epithelial cells	[41-43]
Ki-67	Proliferation	Increased expression in nuclei of metaplastic cells	[44,45]
NF-κB p65	Inflammation	Nuclear translocation	[46,47]
COX-2	Inflammation	Overexpression in epithelial and stromal cells	[48,49]
CD68	Macrophages	Stromal density and phenotype of macrophages	[50,51]
CD45RO	Memory lymphocytes	Stromal density	[52,53]
CD1a	Dendritic cells	Stromal density	[54,55]
HIF-1α	Angiogenesis	Expression and subcellular localization in stromal cells	[56,57]
Cytokeratin-20	Metaplasia	Plasma membrane expression in epithelial cells	[58]
CDX-2	Metaplasia	Nuclear expression in epithelial cells	[59]
Hoechst	DNA label	DNA content, nuclear morphology	[60,61]

BE: Barrett's esophagus, HER2: Human epidermal growth factor receptor 2, AMACR: Alpha-methylacyl-coenzyme A racemase, NF-κB: Nuclear factor kappa-B, COX-2: Cyclooxygenase-2, HIF-1α: Hypoxia-inducible factor-1 alpha

then with 5% goat serum blocking buffer followed by incubation with a primary antibody cocktail containing (i) anti-CK-20, anti-Ki-67, and anti-β-catenin; (ii) anti-p16, anti-AMACR, and anti-p53; (iii) anti-HER2/neu, anti-CK-20, and anti-CDX-2; (iv) CD68, NF-κB p65, and anti-COX2; or (v) anti-HIF-1α, anti-CD45RO and anti-CD1a antibodies for 1 h at room temperature. Antibody sources are detailed in Supplemental Table 1. Slides were washed and incubated for 1 h at room temperature with a secondary antibody cocktail containing Alexa Fluors 488-, 555- and 647-conjugated goat-anti isotype-specific mouse and goat anti-rabbit IgG antibodies (Life Technologies), which were specific to each primary antibody cocktail. Slides were washed, labeled with Hoechst 33342 (Life Technologies) for 3 min, washed again, and mounted with a glass coverslip using Prolong Gold Antifade (Life Technologies).

Whole Slide Scanning

H&E-stained slides were imaged at ×20 magnification on a NanoZoomer Digital Pathology scanner (Hamamatsu Photonics, K.K., Japan). Fluorescently-labeled slides were imaged by whole slide 4-channel fluorescence scanning at ×20 magnification on a ScanScope FL (Aperio Technologies/Leica BioSystems, Vista, CA) utilizing a BrightLine® Pinkel quadband filter set optimized for 4',6-diamidino-2-phenylindole, fluorescein isothiocyanate, tetramethylrhodamine, and Cy5 (FF01-440/521/607/700-25), and BrightLine® single-band bandpass excitation filters FF01-387/11-25, FF01-485/20-25, FF01-560/25-25, and FF01-650/13-25 (Semrock, Rochester, NY, USA). A light source calibration device was utilized to ensure the consistent illumination necessary for quantitative image analysis (Lumen Dynamics/Excelitas Technologies Corp., Waltham, MA). A standardized imaging protocol was developed with optimal exposure times for each channel.

TissueCypher™ Image Analysis Platform

Whole slide fluorescence images were analyzed using Cernostics' TissueCypher™ Image Analysis Platform (Cernostics, Inc., Pittsburgh, PA), which includes a high performance file reading mechanism based on BigTiff format to decode raw image data, MatLab algorithms for segmenting low level tissues objects such as nuclei, cytoplasm, plasma membrane, and whole cells to allow feature collection at the cellular and sub-cellular level and also higher order computer vision models for spatial quantification of biomarkers in tissue compartments, such as epithelium, metaplastic areas, and lamina propria.

Tissue detection

A tissue detection algorithm was developed to detect individual tissue fragments on the slide. This algorithm first converts the four channel tissue image to RGB via R = 485 nm channel plus 650 nm channel, G = 560 nm channel plus 650 nm channel, B = 387 nm channel, then performs image thresholding using Otsu's method[62] and applies a morphological dilate operation followed by a flood-fill operation.

Cellular object segmentation

A nuclei segmentation algorithm was used to generate nuclei masks based on anisotropic diffusion and morphological image processing operations; two-dimensional anisotropic was used,[63] followed by histogram equalization[64] and conversion to binary using Otsu's method. A cell mask was utilized to segment cells containing nuclei by first creating a distance map to which the watershed operation[65] was applied, and then connected components labeling[66] was performed. A cytoplasm mask was generated by subtracting the nuclei mask from the cell mask. Plasma membrane masks were generated using two-dimensional anisotropic diffusion, histogram equalization, and the conversion to binary using a biomarker signal. A nuclei cluster mask was developed based on Gaussian smoothing in the Hoechst channel, rank order filter,[66] image threshold using Otsu's method, morphological operations to remove small objects followed by connected components labeling. Autofluorescence was reduced by removal of overlapping signal above 312.5 (in 10 bit tissue image) in the Alexa Fluor 488 and 555 channels.

Computer vision models for tissue structure segmentation

A metaplastic cell mask for BE was developed based on CK-20 signal. Histogram equalization was performed on CK-20 signal followed by Gaussian smoothing, rank order filter, anisotropic diffusion, image threshold using Otsu's method, and morphological image closing operation, which is a dilation followed by an erosion using the same flat, disk-shaped structuring element.[67] A metaplastic nuclei mask was derived by masking nuclei within the metaplastic cell mask. An epithelial cell mask was developed based on β-catenin plasma membrane signal. Histogram equalization was performed on β-catenin signal followed by Gaussian smoothing, rank order filter, anisotropic diffusion, image threshold using Otsu's method, and a morphological image closing operation. An epithelial nuclei mask was derived by masking nuclei within the epithelial cell mask. A lamina propria mask was generated by subtracting the metaplastic cell mask, and the epithelial cells mask from the whole tissue area. A nuclei cluster mask was developed by Gaussian smoothing of the Hoechst signal, then rank order filter, Otsu's image thresholding, morphological operations to remove small objects (image open (erosion followed by a dilation using the same structuring element[68]), close (dilation followed by an erosion using the same structuring element[67]) and dilate using a flat, disk-shaped structuring element[69]) and finally connected components labeling.

Quantitative biomarker and morphology feature measurements

TissueCypher™ Image Analysis Platform was used to measure an array of features of biomarkers and morphology within segmented cellular objects and segmented tissue structures. Biomarker features included: (i) Basic pixel intensity features (mean, sum, standard deviation, moment), (ii) pixel intensity ratio features (ratio of a biomarker in different subcellular compartments, ratio of one biomarker to another in the same or a different subcellular compartment), and (iii) Haralick texture features (correlation, difference entropy, difference variance, energy, entropy, information measures of correlation, inverse difference moment, sum average, sum entropy, sum of variances, sum variance).[70] Nuclei morphology features included object area, equivalent diameter, solidity, eccentricity, and were applied to all individual nuclei in tissue fragments and nuclei within metaplastic masks and epithelial masks within tissue fragments. Extracted image analysis features were summarized as multiple measures, including percentiles (5^{th}, 15^{th}, 25^{th}, 50^{th}, 75^{th}, 85^{th}, 90^{th}, 95^{th}, and 97^{th}), interquartile range and area under the curve. Threshold-based features were calculated using Boolean filters on the cell object-based features. Features were summarized on the population of cell-objects passing through the Boolean filters, e.g., nuclear area was quantified on cells with nuclei p53 mean intensity >95 and cell p16 mean intensity <100 (on a scale of 0–1023 in the 10 bit tissue images). Features were also localized to rectangular regions (161 × 161 pixels) of tissue images to create microenvironment-based features. These features were summarized to quantify the cell-based biomarker characteristics described above in the top scoring 5 or less microenvironments and the top scoring 5% of microenvironments on each slide.

RESULTS

TissueCypher™ image processing and image analysis algorithms were developed to decode raw image data from multi-channel whole slide fluorescence slides, detect tissue fragments on slides, apply masks to segment subcellular compartments and tissue compartments as individual objects, and calculate multiple biomarker features and morphological features within the segmented cellular and tissue compartments. The TissueCypher Image Analysis Platform is potentially scalable to any tissue biomarker, since it calculates an array of intensity and morphologic features within each type of segmented object (cell, nuclei, cytoplasm, plasma membrane), and to segmented objects within computer vision masks such as epithelial and stromal tissue compartments. These algorithms were used to assess a panel of 14 biomarkers with known diagnostic significance in BE in a set of BE biopsies with GI subspecialist-confirmed diagnoses of nondysplastic BE with RA (RA, n = 22) and BE with HGD (HGD, n = 17). The RA cases were from patients with at least 4 years of endoscopic surveillance data showing no disease progression, and the HGD cases were from patients with subsequent disease progression. The panel of biomarkers evaluated is summarized in Table 1 and includes epithelial-type biomarkers as well as biomarkers of stromal processes, including immune cell subsets. The goal was not to discover novel biomarkers; the goal was to select a panel of well-established biomarkers to demonstrate the ability of the TissueCypher Image Analysis Platform to detect systems molecular and cellular changes between different disease states. Serial sections of FFPE BE biopsies were fluorescently immunolabeled for multiple epithelial and stromal biomarkers (3 per slide) with Hoechst labeling of DNA and imaged by whole slide fluorescence scanning. Example images of 14 biomarkers and DNA labeled in BE biopsies are shown in Figure 1. Whole slide fluorescence images were read into the TissueCypher™ image analysis platform, and individual BE biopsy fragments were identified using the automated tissue detection algorithm [Figure 2]. Cell segmentation masks were applied to the detected biopsy fragments to segment individual nuclei, whole cells, cytoplasm, and plasma membrane [Figure 3]. Tissue structure masks were applied to segment epithelial cells, metaplastic cells, and lamina propria within the biopsy fragments [Figure 4].

Biomarker and morphology features were extracted and evaluated in the confirmed BE HGD cases versus the nondysplastic BE cases with RA. Multiple image analysis features showed significant differences between HGD and RA [Figure 5]. Increases in p53 nuclear intensity, a nuclear area in cells with p53 overexpression and p16 loss and nuclear DNA content were observed in HGD versus RA [Figure 5a-c]. Microenvironments of strong epithelial AMACR expression, stromal cells expressing HIF-1α and CD68 (a macrophage marker) in nuclei clusters in the lamina propria distinguished HGD from RA [Figure 5d-f].

Nuclear Ki-67 signal intensity and nuclear area were evaluated in cells within the metaplasia mask produced by the image analysis. The image analysis features that were evaluated utilized multiple registered channels of tissue image data, including CK-20 to mask the metaplastic tissue compartment, nuclear Ki-67 to assess proliferation and nuclear Hoechst to segment nuclei as individual objects and to calculate nuclei area. Higher levels of proliferation and increased the nuclear area within metaplastic cells were observed in HGD biopsies compared to nondysplastic biopsies with RA [Figure 6].

Combinations of epithelial and stromal cell biomarkers were evaluated in whole slide analyses of cells within BE biopsies. Dysplastic cells in BE frequently overexpress p53

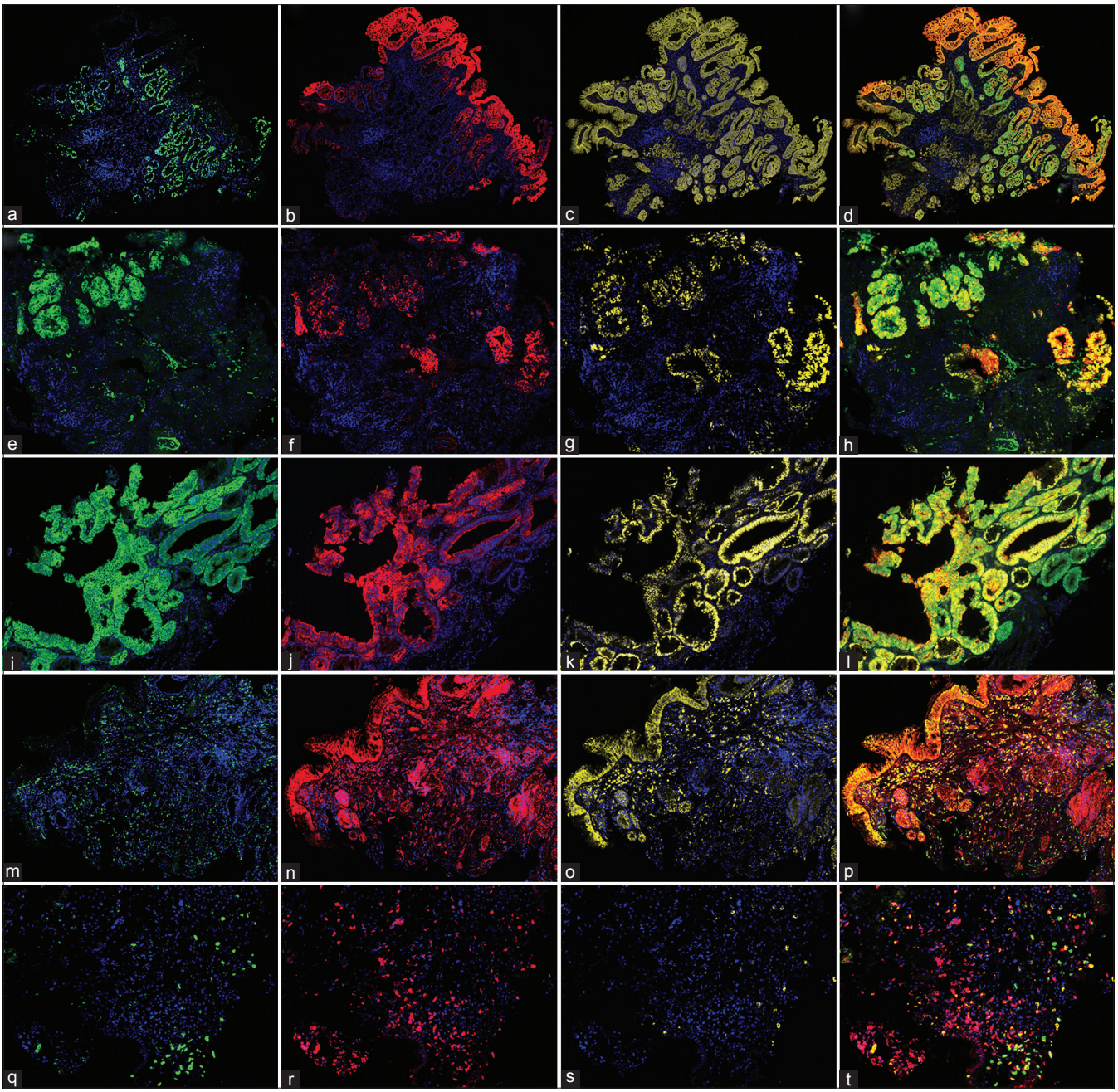

Figure 1: Multiplexed panels of tissue system biomarkers. (a-d) Ki-67 (green), cytokeratin 20 (red), beta-catenin (yellow) and overlay of Ki-67, cytokeratin 20 and beta-catenin. (e-h) p16 (green), alpha-methylacyl-coenzyme A racemase (red), p53 (yellow) and overlay of p16, alpha-methylacyl-coenzyme A racemase and p53. (i-l) human epidermal growth factor receptor 2/neu (green), cytokeratin 20 (red), CDX-2 (yellow) and overlay of human epidermal growth factor receptor 2/neu, cytokeratin 20 and CDX-2. Panels (m-p) CD68 (green), nuclear factor kappa-B p65 (red), COX-2 (yellow) and overlay of CD68, nuclear factor kappa-B and COX-2. (q-t) hypoxia-inducible factor-1 alpha (green), CD45RO (red), CD1a (yellow) and overlay of hypoxia-inducible factor-1 alpha, CD45RO, and CD1a. Hoechst labeling is shown in blue

protein as a result of point mutations that inactivate the protein and slow the rate of p53 degradation, leading to its nuclear accumulation.[34] Loss of p16 protein expression is common in BE and is due to mutation and genomic loss of the p16 gene. Our analysis showed that p53 accumulation and p16 loss occurs in the same cells that p53 accumulation and p16 loss occurred in the same cells [Figure 7a-b, e and f]. Analysis of CD45RO and HIF-1α in the same biopsies revealed heavy infiltration of the lamina propria by $CD45RO^+$ memory lymphocytes and cells expressing HIF-1α in HGD, versus relatively low density of $CD45RO^+$ and HIF-1α-expressing stromal cells in the nondysplastic biopsy with RA [Figure 7c,d, g and h].

A biopsy of BE is a heterogeneous sample that includes normal tissue and a mixed sample of Barrett's mucosa. It

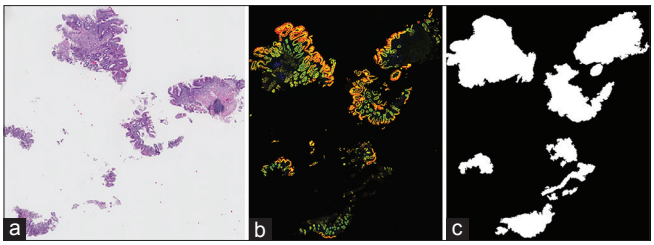

Figure 2: Automated detection of Barrett's esophagus biopsies by TissueCypher Image Analysis Platform. Sections of formalin-fixed paraffin-embedded Barrett's biopsies were stained with H&E and scanned at ×20 (a). Additional sections from the same tissue blocks were fluorescently immunolabeled for Ki-67 (green), cytokeratin 20 (red), beta-catenin (yellow) plus Hoechst labeling of nuclei and scanned at ×20 (b). Whole slide fluorescence images were read into the TissueCypher image analysis software to decode raw image data and detect individual tissue fragments (c)

is well described that epithelial dysplasia can be limited to focal areas on the tissue slide,[71] which underscores the need to consider features limited to small areas or "microenvironments" of a biopsy. Microenvironment-based image analysis features were evaluated to capture focal epithelial abnormalities and clusters of stromal cells in the lamina propria that may be associated with dysplasia in BE. Cell object-based features (i.e., biomarker and morphology features localized to nuclear, cytoplasm, plasma membrane, or whole cell) were localized to discrete regions of the whole slide images to create microenvironment-based features. Alpha-methylacyl-CoA racemase (AMACR) is involved in degradation of branched-chain fatty acids. AMACR expression has been shown to be a specific marker in differentiating HGD from nondysplastic BE.[41,42] The scoring system for AMACR by IHC follows a standard 0–3+ system, in which a score is assigned based on the percentage of epithelial cells expressing the biomarker.[41,43] Although, the scoring system does take into account the heterogeneity of epithelial AMACR expression, this manual scoring system is subject to observer variability and does not take into account its co-expression patterns with other biomarkers. A TissueCypher microenvironment AMACR feature was evaluated in the set of HGD and RA BE cases. The standard deviation of AMACR cellular intensity in tissue microenvironments, reflecting heterogeneous and localized high expression was significantly higher in HGD versus RA biopsies [Figure 5d]. Heat maps of this feature in tissue images demonstrated microenvironments of strong AMACR signal in HGD compared to RA biopsies [Figure 8 a-i]. Multivariate analysis of AMACR, p16, and p53 within the same tissue showed a population of cells within the HGD biopsy with strong AMACR expression. A subset of the AMACR$^+$ cells showed loss of p16 and a subset had a moderate overexpression of p53.

DISCUSSION

Despite advances in other technologies such as DNA microarrays and massively parallel sequencing, anatomic

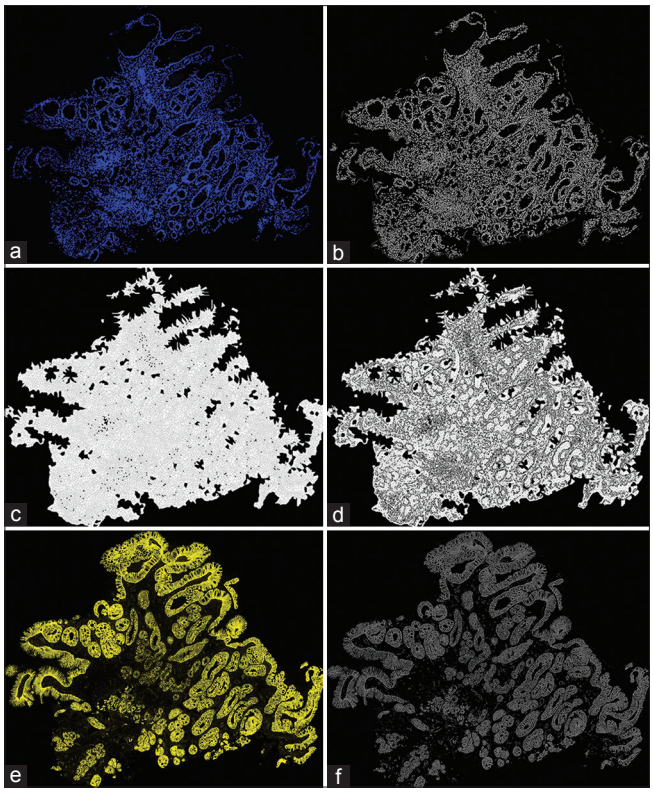

Figure 3: Cellular object segmentation with TissueCypher Image Analysis Platform. TissueCypher performs cellular object segmentation based on the Hoechst channel (a). Individual nuclei, cells, and cytoplasm are segmented (b-d). Plasma membrane segmentation is based on signals from biomarkers that are expressed in the plasma membrane such as beta-catenin in resting state or cytokeratins (e and f). Biomarker and morphology feature measurements are made within these segmented cellular object masks

pathology and microscopic analysis remains the most informative and widely utilized technology for diagnosis and decision-making for cancer patients and patients in cancer screening programs. Although there is a long history of success with regard to manual microscopic diagnosis, there remain areas of well-documented diagnostic uncertainty as in the case of evaluating dysplasia in BE specimens. It is in areas of morphologic uncertainty such as this that the utility of the classic microscopic method can be enhanced by the addition of newer technologies. Additional sections taken from the same FFPE tissue blocks used for routine pathology can be used for multiplexed fluorescence biomarker labeling and quantitative image analysis, revealing molecular and cellular differences that may not be evident with the traditional methods of H&E slides and single marker IHC with manual interpretation.

Setting the stage for the possibility of image analysis as a diagnostic tool is the proliferation of digital imaging platforms for pathology in recent years that continues to gain traction. Improvements to the digital workflow have been shown to enhance the pathologist's user experience.[72] Advances in tissue image color normalization and algorithms

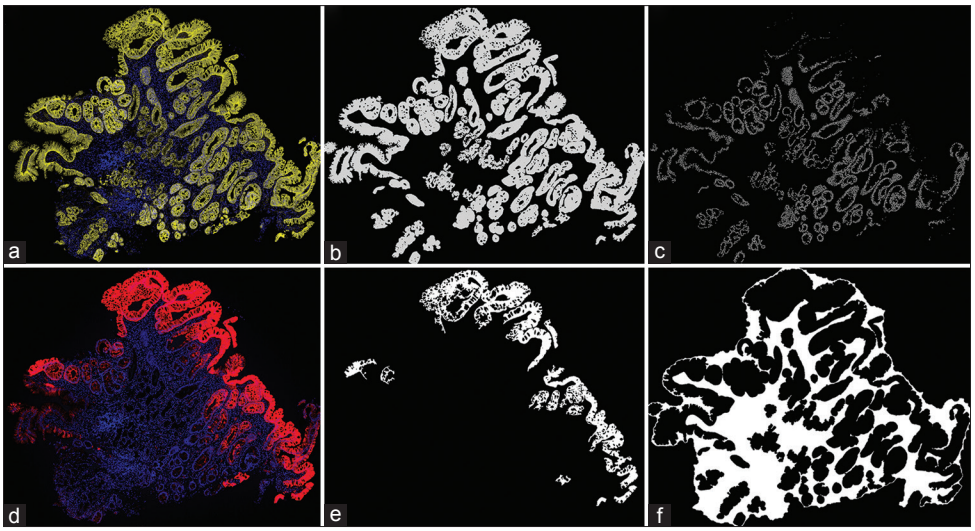

Figure 4: Tissue structure segmentation by TissueCypher Image Analysis Platform. TissueCypher segments Barrett's esophagus fragments into structural compartments to enable contextual measurements of biomarkers and morphology. An epithelial cell mask utilizes beta-catenin signal (a) to segment epithelial cells (b). An epithelial nuclei mask is generated by masking nuclei objects within the epithelial mask (c). A metaplastic cell mask utilizes cytokeratin 20 (d) to segment metaplastic epithelium (e). A lamina propria mask is derived by subtracting the metaplastic and epithelial cell masks from the whole tissue area (f)

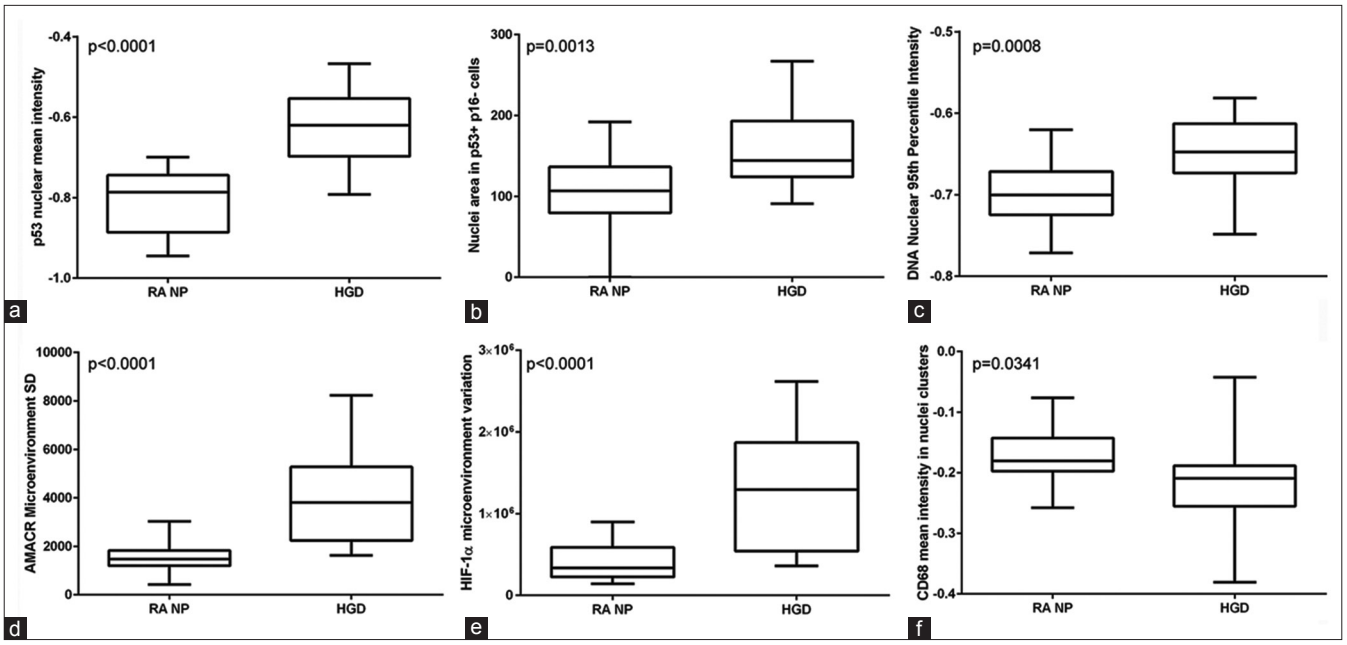

Figure 5: Comparison of TissueCypher quantitative features in Barrett's esophagus biopsies with reactive atypia versus high-grade dysplasia. Box and whisker plots showing image analysis features in Barrett's esophagus biopsies with reactive atypia (*n* = 22) and Barrett's esophagus biopsies with high-grade dysplasia (*n* = 17). (a) p53 nuclear mean intensity; (b) nuclear area in $p53^{+}$ $p16^{-}$ cells; (c) DNA nuclear 95th percentile intensity; (d) alpha-methylacyl-coenzyme A racemase microenvironment standard deviation; (e) hypoxia-inducible factor-1 alpha microenvironment variation; (f) CD68 (macrophages) mean intensity in nuclei clusters. *P* values on each panel are from unpaired *t*-tests comparing the mean of the features in the high-grade dysplasia versus reactive atypia biopsies. Error bars show minimum and maximum values

for the objective assessment of morphology and standard IHC biomarkers will aid adoption of digital imaging in pathology.[8,73-76] The College of American Pathologists Pathology and Laboratory Quality Center has released guidelines for validating whole slide imaging systems for diagnostic purposes, which will further spur implementation of digital pathology into the clinical workflow.[77]

This study specifically evaluated the ability of TissueCypher™ to measure multiple epithelial and stromal biomarkers and nuclear morphology in biopsies of BE with correlation to subspecialist diagnoses of HGD and RA and outcomes of disease progression. A panel of 14 epithelial and stromal biomarkers with known diagnostic and/or prognostic significance in Barrett's

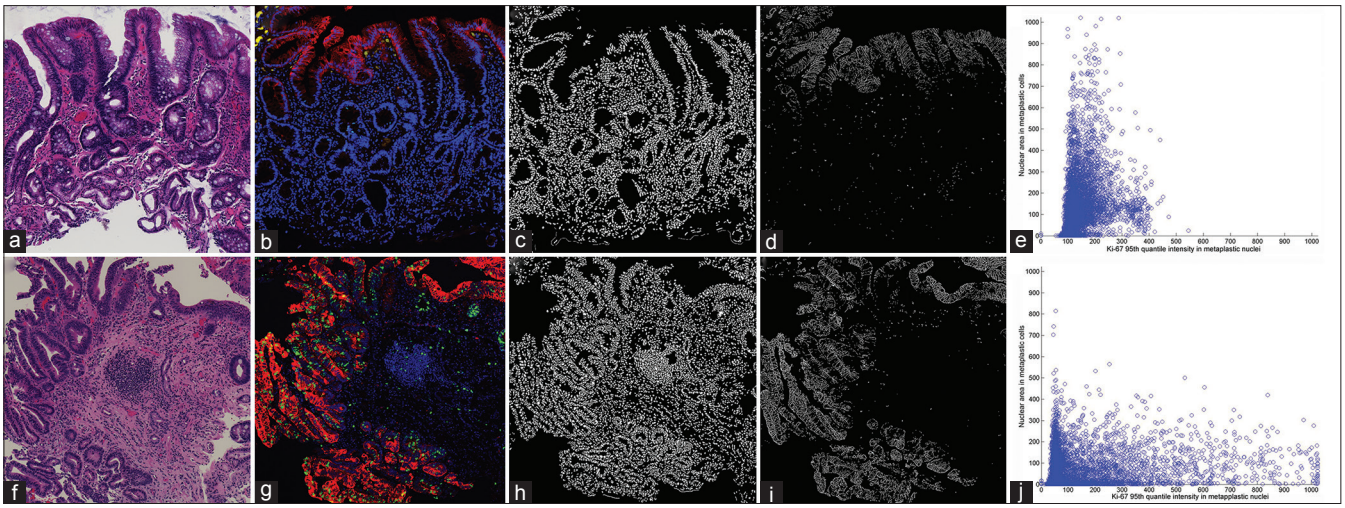

Figure 6: TissueCypher detection of differences in proliferation and morphology in reactive atypia and the high-grade dysplasia biopsies. Barrett's esophagus biopsies with reactive atypia or high-grade dysplasia were H&E stained (a, f) or labeled for cytokeratin 20, Ki-67 and Hoechst (b, g), imaged and analyzed by TissueCypher. H&E-stained slides were imaged to assess morphology in the reactive atypia (a) and high-grade dysplasia (f) biopsies. The reactive atypia patient had 4 years surveillance showing no progression. The high-grade dysplasia patient was diagnosed with esophageal adenocarcinoma 100 days later. Nuclei masks (c, h) and cytokeratin 20 plasma membrane masks (d, i) are shown. Metaplastic cell proliferation and nuclear area were increased in the high-grade dysplasia (g-j) versus reactive atypia biopsy (b-e)

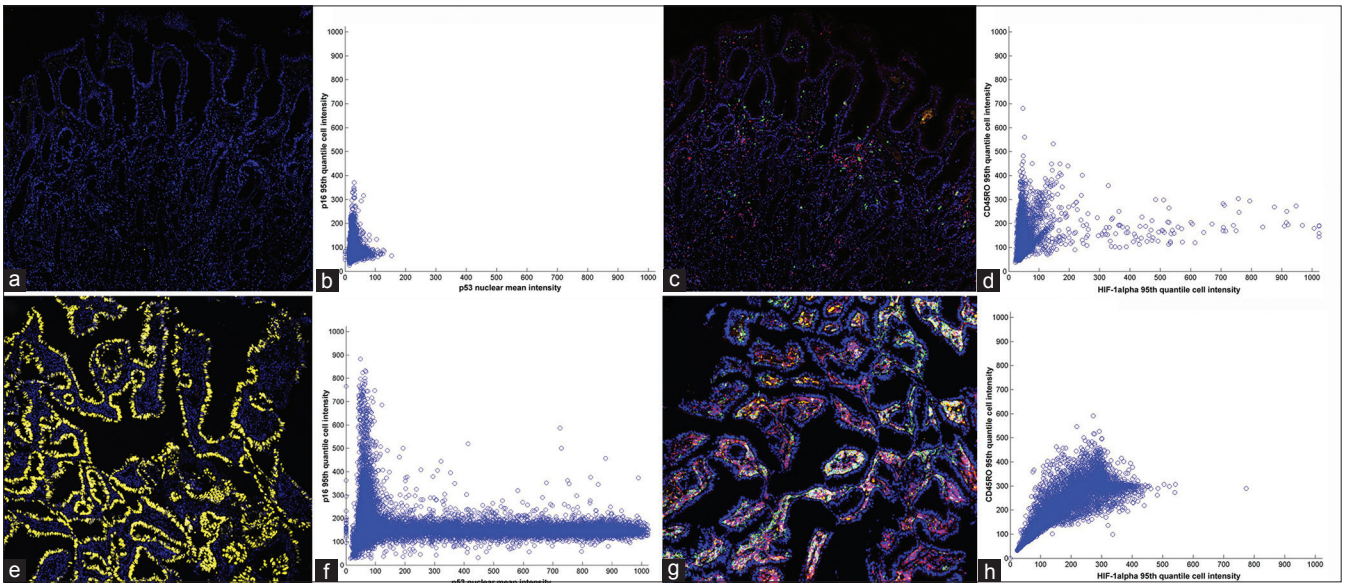

Figure 7: TissueCypher detection of molecular and cellular changes in high-grade dysplasia versus reactive atypia. Biopsies with reactive atypia or high-grade dysplasia were labeled for p16, alpha-methylacyl-coenzyme A racemase, p53 or CD45RO, hypoxia-inducible factor-1 alpha, CD1a, plus Hoechst, imaged and analyzed by TissueCypher. Low p53 levels were detected in reactive atypia (a) whereas diffuse high p53 was detected in high-grade dysplasia (e). The bivariate analysis in reactive atypia (b) and high-grade dysplasia (f) biopsies showed that the majority of p53-high cells had a p16 loss in high-grade dysplasia. Analysis of CD45RO (red) and hypoxia-inducible factor-1 alpha (green) in the same biopsies showed low density of CD45RO$^+$ cells and hypoxia-inducible factor-1 alpha$^+$ cells in reactive atypia (c, d) versus high density in high grade dysplasia (g, h)

was evaluated. The biomarkers included markers of epithelial cell abnormalities known to occur in the malignant progression of BE and also stromal biomarkers, including markers of angiogenesis and immune cell subsets that play roles in cancer development. The TissueCypher technology captured multiple molecular and cellular differences between HGD and RA that may not be evident on H&E slides and/or are difficult to assess by single marker IHC with manual interpretation. Multiple image analysis features derived from epithelial and stromal biomarkers and also nuclear morphology showed different levels in biopsies with HGD versus nondysplastic biopsies with RA. The biomarkers include markers of epithelial cell abnormalities known to occur in the malignant progression of BE such as p16, p53 and AMACR,[42,78,79] and also stromal biomarkers like HIF-1α. Microenvironments of cells expressing HIF-1α were found

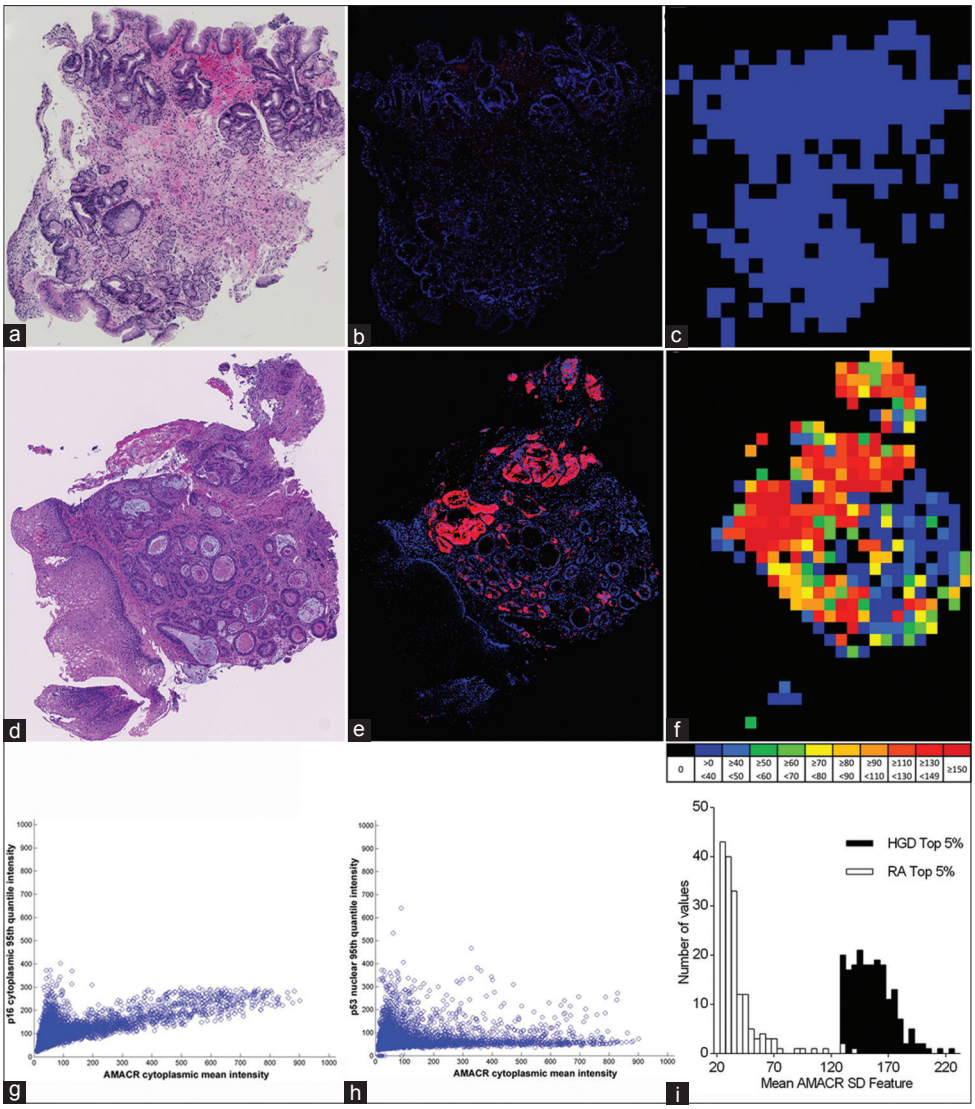

Figure 8: TissueCypher assessment of microenvironment-based biomarker features. Panels (a and d) show H&E, (b and e) alpha-methylacyl-coenzyme A racemase (red) and Hoechst (blue) and (c and f) heat maps of alpha-methylacyl-coenzyme A racemase cell intensity standard deviation in microenvironments in reactive atypia and high grade dysplasia biopsies, respectively. Multivariate analysis showed a population of cells within the high-grade dysplasia biopsy with high alpha-methylacyl-coenzyme A racemase, including a subset with the p16 loss (g) and a p53-high subset (h). Evaluation of the top 5% of alpha-methylacyl-coenzyme A racemase microenvironments showed high levels in the high-grade dysplasia versus reactive atypia biopsy (i)

in biopsies with HGD but not in RA, indicating that in addition to assessing epithelial features, assessment of stromal processes such as angiogenesis can aid in the diagnosis and prognosis of BE.

The quantitative fluorescence approach employed by the TissueCypher™ Image Analysis Platform carries distinct advantages over transmitted light immunohistochemical methods by providing higher resolution linear labeling of multiplexed biomarkers. This technique consumes less of the biopsy tissue by imaging multiple biomarkers in separate fluorescence channels on each slide. The ability to measure multiple biomarkers in spatially overlapping fluorescence channels enables assessment of co-localization of biomarkers of diagnostic and prognostic importance such as the co-expression of Ki-67 and CK20 in proliferating metaplastic tissue and to assess nuclear morphology in populations of cells defined by expression of multiple biomarkers, e.g., cells with p16 loss and p53 overexpression.

The limitations of this study include the retrospective nature of the cohort, which can result in selection bias. The cohort included patients in surveillance at academic referral centers and community practice centers and the biopsies tested were had collection dates spanning a 10-year period, which prevented standardization of biopsy fixation and storage protocols. However, the biopsies were all collected during endoscopic surveillance and thus reflect routine BE samples requiring a risk assessment.

Gene, expression profiling tests and DNA sequencing approaches, have been developed for cancer diagnostics.

These technologies have a significant disadvantage in that they require tissues to be digested to extract nucleic acids for testing. This results in loss of cellular morphology and spatial relationships, which as shown here to relate to diagnosis and outcome. Furthermore, it is clear that both genetic and nongenetic heterogeneity occur in tumors,[80] implying the need for a spatial systems biology approach to cancer diagnostics that measures multiple biomarkers in the appropriate subcellular compartment in the context of tissue architecture.

The TissueCypher Image Analysis Platform is potentially scalable to any tissue biomarker since it calculates an array of intensity and morphologic features within each type of segmented object (cell, nuclei, cytoplasm, plasma membrane) and to segmented objects within computer vision masks such as epithelial and stromal tissue compartments. Quantitative image analysis of systems biomarkers within the appropriate subcellular compartment and tissue structures has many potential clinical applications. The expression, tissue localization, subcellular localization, and ratio of biomarkers between different tissue and cellular compartments are relevant to their diagnostic, prognostic and/or predictive significance. For example the subtypes and spatial distribution of immune cells in tumor-draining lymph nodes are correlated with clinical outcome in breast cancer, and quantitative approaches to biomarker analysis can aid in the understanding of these tissue profiles.[81-83] The subtypes and distributions of immune cell subsets in primary tumors have also been shown to have prognostic and predictive significance.[52,84] The ability to collect an array of features within cellular objects and tissue structures enables extraction of high-dimensional biomarker and morphology data from tissues, which can be mined for signatures associated with diagnosis, prognosis, and responses to therapies. Multivariable classifiers can be utilized to integrate quantitative biomarker and morphology data with relevant clinical variables to produce actionable diagnostic, prognostic, and predictive scores.

In addition to applications in aiding diagnosis of BE as described here, the TissueCypher technology may have applications in predicting future risk of malignant progression in BE. Despite extensive screening programs aimed at preventing EAC, the incidence of this cancer continues to rapidly increase and survival rates remain extremely poor.[85,86] EAC can be effectively prevented if dysplasia is detected and treated early with measures such as radiofrequency ablation (RFA) and endoscopic mucosal resection (EMR).[87,88] The challenge is to identify patients at high risk for disease progression so that treatments such as RFA and EMR can be appropriately targeted to reduce the incidence and mortality of EAC and to improve the cost-effectiveness of the treatments and screening programs. Biomarkers have been described to have prognostic significance in predicting future risk of progression to EAC.[33,89] However, there is no single biomarker that can accurately predict risk for EAC. A multivariable, objective approach that quantifies epithelial and stromal processes will likely improve upon current histologic methods by detecting high-risk molecular and cellular changes that precede the morphologic changes that are evaluated by histopathology.[90]

In summary TissueCypher™ is a quantitative, multiplexed biomarker-morphology imaging approach that enables measurement of multiple key biomarkers in the context of tissue morphology. The ability to multiplex biomarkers and measure relationships between biomarkers and spatial distributions of biomarkers enables a systems biology approach to anatomic pathology in which key epithelial and stromal biomarkers, including immune biomarkers, can be quantified in the context of tissue morphology. This approach was utilized to detect statistically significant differences between BE biopsies with HGD and nondysplastic biopsies with RA. These findings demonstrate the potential of the technology as an addition to standard histopathology in the diagnosis of BE, particularly in distinguishing HGD from RA, which show histologic similarities but are distinct at the molecular and cellular level and require different clinical management. The assessment of epithelial cell abnormalities, such as changes in p53 and p16 protein levels resulting from mutations, combined with assessment of cellular changes such as infiltration of immune cell subsets and angiogenesis in the lamina propria, may serve as an adjunct to conventional pathology in the assessment of BE risk.

Acknowledgments

We thank Georgian Noll and Matthew Barley (Geisinger) for assistance with retrieval of specimens and clinical data.

Financial Support and Sponsorship

This work was supported by a grant from the Pennsylvania Department of Health CURE Program Grant, Research on Cancer Diagnostics or Therapeutics with Commercialization Potential RFA#10-07-03 (J.W.P., J.D., R.J.C-T), a Qualifying Therapeutic Discovery Project Grant, Internal Revenue Service/Affordable Care Act 2010, (R.J.C-T) and by Cernostics, Inc.

Conflicts of Interest

Lia Reese, D. Lansing Taylor and Rebecca Critchley-Thorne hold equity ownership or stock options in Cernostics and Bruce Campbell, Kathleen Repa, Lia Reese, Xuan Mai Nguyen and Rebecca Critchley-Thorne are or were employed by Cernostics, Inc, the commercial entity that developed the proprietary TissueCypher™ technology. Bruce Campbell and Rebecca Critchley-

Thorne report being inventors on a patent application for the TissueCypher™ technology used in this study. Rebecca Critchley-Thorne and D. Lansing Taylor are founders of Cernostics, Inc.

REFERENCES

1. Onega T, Weaver D, Geller B, Oster N, Tosteson AN, Carney PA, *et al.* Digitized whole slides for breast pathology interpretation: Current practices and perceptions. J Digit Imaging 2014;27:642-8.
2. Nederlof M, Watanabe S, Burnip B, Taylor DL, Critchley-Thorne R. High-throughput profiling of tissue and tissue model microarrays: Combined transmitted light and 3-color fluorescence digital pathology. J Pathol Inform 2011;2:50.
3. Pantanowitz L, Valenstein PN, Evans AJ, Kaplan KJ, Pfeifer JD, Wilbur DC, *et al.* Review of the current state of whole slide imaging in pathology. J Pathol Inform 2011;2:36.
4. Dobson L, Conway C, Hanley A, Johnson A, Costello S, O'Grady A, *et al.* Image analysis as an adjunct to manual HER-2 immunohistochemical review: A diagnostic tool to standardize interpretation. Histopathology 2010;57:27-38.
5. Di Cataldo S, Ficarra E, Macii E. Computer-aided techniques for chromogenic immunohistochemistry: Status and directions. Comput Biol Med 2012;42:1012-25.
6. Yeh FC, Parwani AV, Pantanowitz L, Ho C. Automated grading of renal cell carcinoma using whole slide imaging. J Pathol Inform 2014;5:23.
7. Mousavi HS, Monga V, Rao G, Rao AU. Automated discrimination of lower and higher grade gliomas based on histopathological image analysis. J Pathol Inform 2015;6:15.
8. Dennis J, Parsa R, Chau D, Koduru P, Peng Y, Fang Y, *et al.* Quantification of human epidermal growth factor receptor 2 immunohistochemistry using the Ventana Image Analysis System: Correlation with gene amplification by fluorescence *in situ* hybridization: The importance of instrument validation for achieving high (>95%) concordance rate. Am J Surg Pathol 2015;39:624-31.
9. FDA, 501(k) Summary of Substantial Equivalence #K071128, ScanScope XT System with HER2 IHC Image Analysis Application, Aperio Technologies, Inc.; 2007. Available from: hhttp://www.accessdata.fda.gov/cdrh_docs/reviews/K071128.pdf. [Last accessed on 2015 May 18].
10. FDA, 510(k) Substantial Equivalence Determination Decision Summary #K130515, Virtuoso System for IHC ER (SPI), Ventana Medical Systems, Inc.; 2013. Available from: https://www.accessdata.fda.gov/scripts/cdrh/cfdocs/cfpmn/pmn.cfm?ID=K130515. [Last accessed on 2015 May 18].
11. Critchley-Thorne RJ, Miller SM, Taylor DL, Lingle WL. Applications of cellular systems biology in breast cancer patient stratification and diagnostics. Comb Chem High Throughput Screen 2009;12:860-9.
12. Gough A, Lezon T, Faeder J, Chennubhotla C, Murphy R, Critchley-Thorne R, *et al.* High content analysis and cellular and tissue systems biology: A bridge between cancer cell biology and tissue-based diagnostics. In: Mendelsohn J, Howley PM, Israel MA, Gray JW, Thompson CB, editors. The Molecular Basis of Cancer. 4th ed. New York: Elsevier; 2014.
13. Gough AH, Giuliano KA, Taylor DL. Method For Automated Tissue Analysis. US Patent 8,114,615, Priority Date: May 17, 2006. Assignee: Cernostics, Inc.
14. Gough AH, Giuliano KA, Taylor DL. Method For Automated Tissue Analysis. US Patent 8,597,899, Priority date: May 17, 2006, Assignee: Cernostics, Inc.
15. Gough AH, Giuliano KA, Taylor DL. Method for Automated Tissue Analysis. Japanese Patent 5406019, Priority date: May 17, 2006, Assignee: Cernostics, Inc.
16. Thorne RJ, Campbell BB. Systems and compositions for diagnosing Barrett's Esophagus and methods of using the same. Patent Application PCT/US2012/029198, Priority date: Mar 17, 2011, Assignee: Cernostics, Inc.
17. Yantiss RK. Diagnostic challenges in the pathologic evaluation of Barrett esophagus. Arch Pathol Lab Med 2010;134:1589-600.
18. Naini BV, Chak A, Ali MA, Odze RD. Barrett's oesophagus diagnostic criteria: Endoscopy and histology. Best Pract Res Clin Gastroenterol 2015;29:77-96.
19. Wani S, Falk G, Hall M, Gaddam S, Wang A, Gupta N, *et al.* Patients with nondysplastic Barrett's esophagus have low risks for developing dysplasia or esophageal adenocarcinoma. Clin Gastroenterol Hepatol 2011;9:220-7.
20. Wani S, Falk GW, Post J, Yerian L, Hall M, Wang A, *et al.* Risk factors for progression of low-grade dysplasia in patients with Barrett's esophagus. Gastroenterology 2011;141:1179-86, 1186.e1.
21. Thota PN, Lee HJ, Goldblum JR, Liu X, Sanaka MR, Gohel T, *et al.* Risk stratification of patients with barrett's esophagus and low-grade dysplasia or indefinite for dysplasia. Clin Gastroenterol Hepatol 2015;13:459-65.e1.
22. American Gastroenterological Association, Spechler SJ, Sharma P, Souza RF, Inadomi JM, Shaheen NJ. American Gastroenterological Association medical position statement on the management of Barrett's esophagus. Gastroenterology 2011;140:1084-91.
23. Reid BJ, Haggitt RC, Rubin CE, Roth G, Surawicz CM, Van Belle G, *et al.* Observer variation in the diagnosis of dysplasia in Barrett's esophagus. Hum Pathol 1988;19:166-78.
24. Montgomery E, Bronner MP, Goldblum JR, Greenson JK, Haber MM, Hart J, *et al.* Reproducibility of the diagnosis of dysplasia in Barrett esophagus: A reaffirmation. Hum Pathol 2001;32:368-78.
25. Phoa KN, van Vilsteren FG, Weusten BL, Bisschops R, Schoon EJ, Ragunath K, *et al.* Radiofrequency ablation vs endoscopic surveillance for patients with Barrett esophagus and low-grade dysplasia: A randomized clinical trial. JAMA 2014;311:1209-17.
26. Small AJ, Araujo JL, Leggett CL, Mendelson AH, Agarwalla A, Abrams JA, *et al.* Radiofrequency ablation is associated with decreased neoplastic progression in patients with Barrett's esophagus and confirmed low-grade dysplasia. Gastroenterology 2015;Epub ahead of print.
27. Odze RD. Diagnosis and grading of dysplasia in Barrett's oesophagus. J Clin Pathol 2006;59:1029-38.
28. Coco DP, Goldblum JR, Hornick JL, Lauwers GY, Montgomery E, Srivastava A, *et al.* Interobserver variability in the diagnosis of crypt dysplasia in Barrett esophagus. Am J Surg Pathol 2011;35:45-54.
29. Binato M, Gurski RR, Fagundes RB, Meurer L, Edelweiss MI. P53 and Ki-67 overexpression in gastroesophageal reflux disease – Barrett's esophagus and adenocarcinoma sequence. Dis Esophagus 2009;22:588-95.
30. Rygiel AM, Milano F, Ten Kate FJ, Schaap A, Wang KK, Peppelenbosch MP, *et al.* Gains and amplifications of c-myc, EGFR, and 20.q13 loci in the no dysplasia-dysplasia-adenocarcinoma sequence of Barrett's esophagus. Cancer Epidemiol Biomarkers Prev 2008;17:1380-5.
31. Barrett MT, Sanchez CA, Galipeau PC, Neshat K, Emond M, Reid BJ. Allelic loss of 9p21 and mutation of the CDKN2/p16 gene develop as early lesions during neoplastic progression in Barrett's esophagus. Oncogene 1996;13:1867-73.
32. Glickman JN, Blount PL, Sanchez CA, Cowan DS, Wongsurawat VJ, Reid BJ, *et al.* Mucin core polypeptide expression in the progression of neoplasia in Barrett's esophagus. Hum Pathol 2006;37:1304-15.
33. Varghese S, Lao-Sirieix P, Fitzgerald RC. Identification and clinical implementation of biomarkers for Barrett's esophagus. Gastroenterology 2012;142:435-41.e2.
34. Reid BJ, Prevo LJ, Galipeau PC, Sanchez CA, Longton G, Levine DS, *et al.* Predictors of progression in Barrett's esophagus II: Baseline 17p (p53) loss of heterozygosity identifies a patient subset at increased risk for neoplastic progression. Am J Gastroenterol 2001;96:2839-48.
35. Bird-Lieberman EL, Dunn JM, Coleman HG, Lao-Sirieix P, Oukrif D, Moore CE, *et al.* Population-based study reveals new risk-stratification biomarker panel for Barrett's esophagus. Gastroenterology 2012;143:927-35.e3.
36. Galipeau PC, Li X, Blount PL, Maley CC, Sanchez CA, Odze RD, *et al.* NSAIDs modulate CDKN2A, TP53, and DNA content risk for progression to esophageal adenocarcinoma. PLoS Med 2007;4:e67.
37. van Dekken H, Hop WC, Tilanus HW, Haringsma J, van der Valk H, Wink JC, *et al.* Immunohistochemical evaluation of a panel of tumor cell markers during malignant progression in Barrett esophagus. Am J Clin Pathol 2008;130:745-53.
38. Moyes LH, McEwan H, Radulescu S, Pawlikowski J, Lamm CG, Nixon C, *et al.* Activation of Wnt signalling promotes development of dysplasia in Barrett's oesophagus. J Pathol 2012;228:99-112.
39. Fritcher EG, Brankley SM, Kipp BR, Voss JS, Campion MB, Morrison LE, *et al.* A comparison of conventional cytology, DNA ploidy analysis, and fluorescence *in situ* hybridization for the detection of dysplasia and adenocarcinoma in patients with Barrett's esophagus. Hum Pathol 2008;39:1128-35.
40. Rossi E, Villanacci V, Bassotti G, Donato F, Festa A, Cengia G, *et al.*

TOPOIIalpha and HER-2/neu overexpression/amplification in Barrett's oesophagus, dysplasia and adenocarcinoma. Histopathology 2010;57:81-9.
41. Lisovsky M, Falkowski O, Bhuiya T. Expression of alpha-methylacyl-coenzyme A racemase in dysplastic Barrett's epithelium. Hum Pathol 2006;37:1601-6.
42. Dorer R, Odze RD. AMACR immunostaining is useful in detecting dysplastic epithelium in Barrett's esophagus, ulcerative colitis, and Crohn's disease. Am J Surg Pathol 2006;30:871-7.
43. Kastelein F, Biermann K, Steyerberg EW, Verheij J, Kalisvaart M, Looijenga LH, *et al.* Value of a-methylacyl-CoA racemase immunochemistry for predicting neoplastic progression in Barrett's oesophagus. Histopathology 2013;63:630-9.
44. Sikkema M, Kerkhof M, Steyerberg EW, Kusters JG, van Strien PM, Looman CW, *et al.* Aneuploidy and overexpression of Ki67 and p53 as markers for neoplastic progression in Barrett's esophagus: A case-control study. Am J Gastroenterol 2009;104:2673-80.
45. Volkweis BS, Gurski RR, Meurer L, Pretto GG, Mazzini Gda S, Edelweiss MI. Ki-67 antigen overexpression is associated with the metaplasia-adenocarcinoma sequence in Barrett's esophagus. Gastroenterol Res Pract 2012;2012:639748.
46. Abdel-Latif MM, O'Riordan J, Windle HJ, Carton E, Ravi N, Kelleher D, *et al.* NF-kappaB activation in esophageal adenocarcinoma: Relationship to Barrett's metaplasia, survival, and response to neoadjuvant chemoradiotherapy. Ann Surg 2004;239:491-500.
47. O'Riordan JM, Abdel-latif MM, Ravi N, McNamara D, Byrne PJ, McDonald GS, *et al.* Proinflammatory cytokine and nuclear factor kappa-B expression along the inflammation-metaplasia-dysplasia-adenocarcinoma sequence in the esophagus. Am J Gastroenterol 2005;100:1257-64.
48. Lagorce C, Paraf F, Vidaud D, Couvelard A, Wendum D, Martin A, *et al.* Cyclooxygenase-2 is expressed frequently and early in Barrett's oesophagus and associated adenocarcinoma. Histopathology 2003;42:457-65.
49. Sonoda R, Naomoto Y, Shirakawa Y, Fujiwara Y, Yamatsuji T, Noma K, *et al.* Preferential up-regulation of heparanase and cyclooxygenase-2 in carcinogenesis of Barrett's oesophagus and intestinal-type gastric carcinoma. Histopathology 2010;57:90-100.
50. Mantovani A, Savino B, Locati M, Zammataro L, Allavena P, Bonecchi R. The chemokine system in cancer biology and therapy. Cytokine Growth Factor Rev 2010;21:27-39.
51. Erreni M, Mantovani A, Allavena P. Tumor-associated Macrophages (TAM) and inflammation in colorectal cancer. Cancer Microenviron 2011;4:141-54.
52. Galon J, Costes A, Sanchez-Cabo F, Kirilovsky A, Mlecnik B, Lagorce-Pagès C, *et al.* Type, density, and location of immune cells within human colorectal tumors predict clinical outcome. Science 2006;313:1960-4.
53. Rauser S, Langer R, Tschernitz S, Gais P, Jütting U, Feith M, *et al.* High number of CD45RO tumor infiltrating lymphocytes is an independent prognostic factor in non-metastasized (stage I-IIA) esophageal adenocarcinoma. BMC Cancer 2010;10:608.
54. Cappello F, Rappa F, Anzalone R, La Rocca G, Zummo G. CD1a expression by Barrett's metaplasia of gastric type may help to predict its evolution towards cancer. Br J Cancer 2005;92:888-90.
55. Bobryshev YV, Tran D, Killingsworth MC, Buckland M, Lord RV. Dendritic cells in Barrett's esophagus and esophageal adenocarcinoma. J Gastrointest Surg 2009;13:44-53.
56. Griffiths EA, Pritchard SA, McGrath SM, Valentine HR, Price PM, Welch IM, *et al.* Increasing expression of hypoxia-inducible proteins in the Barrett's metaplasia-dysplasia-adenocarcinoma sequence. Br J Cancer 2007;96:1377-83.
57. Ling FC, Khochfar J, Baldus SE, Brabender J, Drebber U, Bollschweiler E, *et al.* HIF-1alpha protein expression is associated with the environmental inflammatory reaction in Barrett's metaplasia. Dis Esophagus 2009;22:694-9.
58. Ormsby AH, Goldblum JR, Rice TW, Richter JE, Falk GW, Vaezi MF, *et al.* Cytokeratin subsets can reliably distinguish Barrett's esophagus from intestinal metaplasia of the stomach. Hum Pathol 1999;30:288-94.
59. Moons LM, Bax DA, Kuipers EJ, Van Dekken H, Haringsma J, Van Vliet AH, *et al.* The homeodomain protein CDX2 is an early marker of Barrett's oesophagus. J Clin Pathol 2004;57:1063-8.
60. Fang M, Lew E, Klein M, Sebo T, Su Y, Goyal R. DNA abnormalities as marker of risk for progression of Barrett's esophagus to adenocarcinoma: Image cytometric DNA analysis in formalin-fixed tissues. Am J Gastroenterol 2004;99:1887-94.
61. Choi WT, Emond MJ, Rabinovitch PS, Ahn J, Upton MP, Westerhoff M. Indefinite for dysplasia in Barrett's esophagus: Inflammation and DNA content abnormality are significant predictors of early detection of neoplasia. Clin Transl Gastroenterol 2015;6:e81.
62. Otsu N. A threshold selection method from gray-level histograms. IEEE Trans Syst Man Cybern 1979;9:62-6.
63. Perona P, Malik J. Scale-space and edge detection using anisotropic diffusion. IEEE Trans Pattern Anal Mach Intell 1990;12:629-39.
64. Zuiderveld K. Contrast limited adaptive histogram equalization. In: Heckbert PS, editor. Graphics Gems IV. San Diego, CA: Academic Press Professional, Inc.; 1994. p. 474-85.
65. Beucher S, Lantuéjoul C. Use of Watersheds in Contour Detection. In: Proc. International Workshop on Image Processing. Real-Time Edge and Motion Detection/Estimation, Rennes, France; 1979.
66. Haralick RM, Shapiro LG. Computer and Robot Vision. Vol. 1: Boston, MA: Addison-Wesley Longman Publishing Co., Inc. 1992. p. 28-48.
67. MathWorks. Imclose-Image Processing Toolbox. Natick, MA: MathWorks. Available from: http://www.mathworks.com/help/images/ref/imclose.html#responsive_offcanvas. [Last accessed on 2015 May 18].
68. MathWorks, Imopen-Image Processing Toolbox. Natick, MA: MathWorks. Available from: http://www.mathworks.com/help/images/ref/imopen.html. [Last accessed on 2015 May 18].
69. MathWorks. Imdilate-Image Processing Toolbox. Natick, MA, USA: MathWorks. Available from: http://www.mathworks.com/help/images/ref/imdilate.html. [Last accessed on 2015 May 18].
70. Haralick RM, Shanmugam K, Dinstein I. Textural feature for image classification. IEEE Trans Syst Man Cyber 1973;3:610-21.
71. Dar MS, Goldblum JR, Rice TW, Falk GW. Can extent of high grade dysplasia in Barrett's oesophagus predict the presence of adenocarcinoma at oesophagectomy? Gut 2003;52:486-9.
72. Randell R, Ruddle RA, Thomas RG, Mello-Thoms C, Treanor D. Diagnosis of major cancer resection specimens with virtual slides: Impact of a novel digital pathology workstation. Hum Pathol 2014;45:2101-6.
73. Cooper LA, Kong J, Gutman DA, Wang F, Gao J, Appin C, *et al.* Integrated morphologic analysis for the identification and characterization of disease subtypes. J Am Med Inform Assoc 2012;19:317-23.
74. Khan AM, Rajpoot N, Treanor D, Magee D. A nonlinear mapping approach to stain normalization in digital histopathology images using image-specific color deconvolution. IEEE Trans Biomed Eng 2014;61:1729-38.
75. Balsat C, Signolle N, Goffin F, Delbecque K, Plancoulaine B, Sauthier P, *et al.* Improved computer-assisted analysis of the global lymphatic network in human cervical tissues. Mod Pathol 2014;27:887-98.
76. Feuchtinger A, Stiehler T, Jütting U, Marjanovic G, Luber B, Langer R, *et al.* Image analysis of immunohistochemistry is superior to visual scoring as shown for patient outcome of esophageal adenocarcinoma. Histochem Cell Biol 2015;143:1-9.
77. Pantanowitz L, Sinard JH, Henricks WH, Fatheree LA, Carter AB, Contis L, *et al.* Validating whole slide imaging for diagnostic purposes in pathology: Guideline from the College of American Pathologists Pathology and Laboratory Quality Center. Arch Pathol Lab Med 2013;137:1710-22.
78. Wong DJ, Paulson TG, Prevo LJ, Galipeau PC, Longton G, Blount PL, *et al.* p16(INK4a) lesions are common, early abnormalities that undergo clonal expansion in Barrett's metaplastic epithelium. Cancer Res 2001;61:8284-9.
79. Kastelein F, Biermann K, Steyerberg EW, Verheij J, Kalisvaart M, Looijenga LH, *et al.* Aberrant p53 protein expression is associated with an increased risk of neoplastic progression in patients with Barrett's oesophagus. Gut 2013;62:1676-83.
80. Burrell RA, McGranahan N, Bartek J, Swanton C. The causes and consequences of genetic heterogeneity in cancer evolution. Nature 2013;501:338-45.
81. Kohrt HE, Nouri N, Nowels K, Johnson D, Holmes S, Lee PP. Profile of immune cells in axillary lymph nodes predicts disease-free survival in breast cancer. PLoS Med 2005;2:e284.
82. Setiadi AF, Ray NC, Kohrt HE, Kapelner A, Carcamo-Cavazos V, Levic EB, *et al.* Quantitative, architectural analysis of immune cell subsets in tumor-draining lymph nodes from breast cancer patients and healthy lymph nodes. PLoS One 2010;5:e12420.
83. Chang AY, Bhattacharya N, Mu J, Setiadi AF, Carcamo-Cavazos V, Lee GH,

et al. Spatial organization of dendritic cells within tumor draining lymph nodes impacts clinical outcome in breast cancer patients. J Transl Med 2013;11:242.
84. Brown JR, Wimberly H, Lannin DR, Nixon C, Rimm DL, Bossuyt V. Multiplexed quantitative analysis of CD3, CD8, and CD20 predicts response to neoadjuvant chemotherapy in breast cancer. Clin Cancer Res 2014;20:5995-6005.
85. Pohl H, Welch HG. The role of overdiagnosis and reclassification in the marked increase of esophageal adenocarcinoma incidence. J Natl Cancer Inst 2005;97:142-6.
86. Cancer Facts and Figures. Atlanta, GA: American Cancer Society; 2014.
87. Shaheen NJ, Overholt BF, Sampliner RE, Wolfsen HC, Wang KK, Fleischer DE, *et al.* Durability of radiofrequency ablation in Barrett's esophagus with dysplasia. Gastroenterology 2011;141:460-8.
88. Tomizawa Y, Iyer PG, Wong Kee Song LM, Buttar NS, Lutzke LS, Wang KK. Safety of endoscopic mucosal resection for Barrett's esophagus. Am J Gastroenterol 2013;108:1440-7.
89. Timmer MR, Sun G, Gorospe EC, Leggett CL, Lutzke L, Krishnadath KK, *et al.* Predictive biomarkers for Barrett's esophagus: So near and yet so far. Dis Esophagus 2013;26:574-81.
90. Hoerres M, Critchley-Thorne R. Barrett's esophagus and the need for improved diagnostic and prognostic testing. MLO Med Lab Obs 2014;46:32, 34.

Supplemental Table 1: Primary antibodies

Primary antibody	Vendor	Catalog
AMACR	Dako	M3616
β-catenin	Biocare Medical	CM406A
CD1a	Cell Marque	101M-14
CD45RO	Biocare Medical	CM006B
CD68	Dako	M0876
CDX-2	Invitrogen	39-7800
c-erbB-2 oncoprotein	Dako	A0485
Cytokeratin-20	Dako	M7019
COX-2	Biocare Medical	CRM306A
HIF-1α	Biocare Medical	CME349A
Ki-67	Cell Marque	275R-14
NF-κB p65	Santa Cruz Biotechnology	Sc-372
p16 (JC8)	Santa Cruz Biotechnology	Sc-56330
p53	Dako	M7001

AMACR: Alpha-methylacyl-coenzyme A racemase, COX-2: Cyclooxygenase-2, HIF-1α: Hypoxia-inducible factor-1 alpha, NF-κB: Nuclear factor kappa-B